ACLNet: A Deep Learning Model for ACL Rupture Classification Combined with Bone Morphology

Chao Liu[1,2,3], Xueqing Yu[1,2,3], Dingyu Wang[4,5,6], and Tingting Jiang[1,2,3]

[1] National Engineering Research Center of Visual Technology, School of Computer Science, Peking University, Beijing, China
[2] State Key Laboratory of Multimedia Information Processing, School of Computer Science, Peking University, Beijing, China
[3] National Biomedical Imaging Center, Peking University, Beijing, China
[4] Department of Sports Medicine, Peking University Third Hospital, Institute of Sports Medicine of Peking University, Beijing, China
[5] Beijing Key Laboratory of Sports Injuries, Beijing, China
[6] Engineering Research Center of Sports Trauma Treatment Technology and Devices, Ministry of Education, Beijing, China
{lchao@stu., yuxueqing@, wang_dingyu@, ttjiang@}pku.edu.cn

Abstract. Magnetic Resonance Imaging (MRI) is widely used in diagnosing anterior cruciate ligament (ACL) injuries due to its ability to provide detailed image data. However, existing deep learning approaches often overlook additional factors beyond the image itself. In this study, we aim to bridge this gap by exploring the relationship between ACL rupture and the bone morphology of the femur and tibia. Leveraging extensive clinical experience, we acknowledge the significance of this morphological data, which is not readily observed manually. To effectively incorporate this vital information, we introduce ACLNet, a novel model that combines the convolutional representation of MRI images with the transformer representation of bone morphological point clouds. This integration significantly enhances ACL injury predictions by leveraging both imaging and geometric data. Our methodology demonstrated an enhancement in diagnostic precision on the in-house dataset compared to image-only methods, elevating the accuracy from 87.59% to 92.57%. This strategy of utilizing implicitly relevant information to enhance performance holds promise for a variety of medical-related tasks.

Keywords: ACL Classification · MRI Image Processing · Point Cloud Transformer · Feature Fusion.

1 Introduction

The anterior cruciate ligament (ACL), a pivotal structure within the knee complex, ensures the joint's stability by mitigating excessive anterior displacement of the tibia against the femur and facilitating rotational equilibrium. ACL ruptures, prevalent in both athletic and general populations, incur an estimated

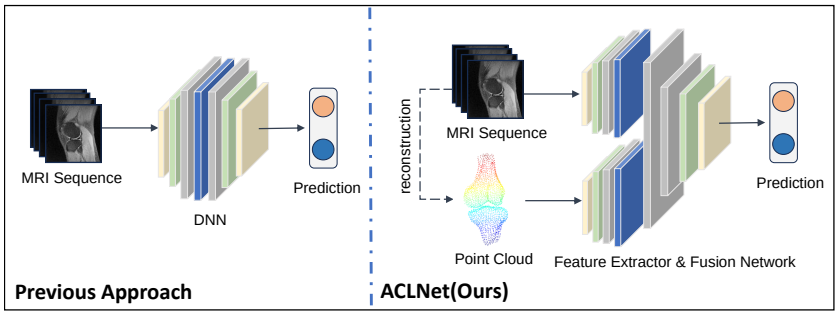

Fig. 1. In comparison to previous methods, our model incorporates bone morphology into the input data.

annual incidence rate of 68.6 per 100,000 person-years [16], precipitating pain, swelling, compromised knee stability, substantial detriment to daily function and life quality, alongside an escalated risk for ensuing osteoarthritis [21]. Consequently, prompt, accurate diagnosis, followed by apt intervention, becomes imperative to preserve knee joint functionality post-ACL rupture.

Magnetic resonance imaging (MRI) stands as the preferred diagnostic modality for ACL injuries, attributed to its high sensitivity and specificity. Nonetheless, the intricate anatomy of the knee, compounded by the requisite for specialized training and variable clinician expertise, renders the accurate interpretation of knee MRIs a daunting, time-intensive endeavor.

Recent forays into deploying deep learning techniques for bolstering ACL injury identification have yielded auspicious outcomes, underscoring the synergy between medical science and artificial intelligence. This confluence has demonstrated that algorithmically extracted features from MRI scans can facilitate robust ACL diagnostics, achieving predictive area under the curve (AUC) metrics ranging from 0.895 to 0.980 [8]. Pioneering studies, such as that by Namiri. et al. [11], have innovated with segmentation networks to delineate ligament territories within MRIs, enhancing classification accuracy through three-dimensional convolutions. Yet, despite these advances, existing models—whether through sophisticated localization or complex convolutional architectures—remain predominantly tethered to analyzing raw MRI imagery, often falling short of expert human diagnostic performance [3, 11, 12, 15, 19].

Given MRI's rich informational content, a strategy that mines MRI features while incorporating crucial supplementary data holds promise for elevating ACL rupture diagnostic precision. Notably, the majority of ACL injuries manifest via non-contact mechanisms [22], suggesting the influence of underlying anatomical predispositions. Clinical observations have correlated certain femoral and tibial morphologies with increased ACL rupture risk [1, 2], prompting the identification of numerous skeletal risk markers—such as femoral notch width and tibial slope—for assessing rupture and surgical failure probabilities [2, 4, 9, 10]. Biomechanical research further corroborates the role of specific bone morpholo-

Table 1. Summary of Subject Demographic and Clinical Data.

Age	Female/male(%)	Rupture/normal(%)	Datasets	
			Train(%)	Validation(%)
31.8±11.2	670/1234(35.2/64.8)	947/957(49.7/50.3)	1521(79.9)	383(20.1)

gies in exacerbating ACL stress, implicating them in the ligament's rupture etiology [7, 18]. Motivated by these etiological insights, we posit that bone morphological characteristics represent a critical, yet underexplored dimension that could significantly augment model diagnostic accuracy to rival or surpass expert levels. Leveraging existing in-house datasets powerd by hospital, we incorporate femoro-tibial boundary annotations, rendered into point clouds, to facilitate transformer-based [17] feature extraction.

We introduce ACLNet, a novel methodology distinctively integrates bone morphological insights as auxiliary diagnostic annotations. This approach encodes morphological nuances elusive to direct expert observation, thereby enhancing classification efficacy. In addition to MRI sequences used to extract image features, we obtained bone morphological point cloud information for each case based on in-house annotated information. We extract image features and point cloud features on two branches respectively. The former captures ACL region's structural and textural essenceInitially while the latter mirroring three-dimensional morphologies. A feature fusion module then synergistically leverages these dual branchs, culminating in substantial classification performance enhancements. Our approach achieves a final classification accuracy of 92.57%, marking a 4.99% improvement over non-morphologically augmented models and comparable to medical expert diagnostic levels.

2 Dataset

To enable a dual-input classification framework analyzing both 2D image sequences and 3D point data, we meticulously curated a novel dataset, denoted as $\mathcal{D} = \{X_i, P_i\}(i = 1, 2...N)(N = 1904)$, which initially comprising 54,008 MRI images. This study protocol(IRB00006761-M2024043) and informed consent exemption were approved by Peking University Third Hospital Medical Science Research Ethics Committee. We built our own dataset due to the lack of MRI acquisition parameters in existing datasets which are necessary for computing spatial point cloud. For the same reason, we only evaluate all the algorithms on our own dataset. The data distribution of different cases is shown in Table 1. Sagittal MRI sequences are utilized for image data, as they provide comprehensive organizational and structural details of the anterior cruciate ligament (ACL), enhancing the model's accuracy in characterizing ACL texture. Additionally, to ensure a comprehensive representation of morphological information, both sagittal and coronal sequences are employed for reconstructing 3D point

cloud data from thick-layer MRI scans. The preparation of the dataset involved several preprocessing steps:

1. 3D MRI image Data: For each case, the original sagittal MRI sequence length vary from 13 to 24, while a slice resolution is 512×512. By undergoing process of selection, cropping, and resizing, we transform the original sequences into uniform $16 \times 112 \times 112$ 3D image data. We use X_i to represent it.
2. Point Cloud Data: Point cloud inputs are derived from the original MRI data, where each slice image is annotated with boundary points identifying the femur and tibia by medical experts. We had 45 doctors involved in data labeling with 2 doctors overseeing the audit. Each doctor received over 4 hours of labeling training. The workflow included an initial labeling round followed by a review round. Along with additional data extracted from the MRI(detailed in the supplementary material), these points are re-positioned into a 3D spatial arrangement that reflects the original point cloud structure. Through farthest point sampling and resampling, each case is represented by a standardized point cloud comprising 2048 points. We use $P_i(i = 1, 2...N)$ to represent it.
3. Clinical imaging report: For each case, there is a radiological report describing the diagnosis of ACL rupture. The clinical imaging reports were written by a radiology resident, verified and signed by two senior radiology attendings. For each case, the diagnosis result of ACL rupture is denoted as $\tilde{y}_i(i = 1, 2...N)$.
4. Ground Truth: The Ground truth was provided by the surgical diagnosis. During the surgery, the surgeon would give the diagnosis of the ACL under direct vision. Labeled as $y_i(i = 1, 2...N)$, we use these diagnosis as ground truth.

Figure 1 provides visual examples of the 3D image data and 3D point cloud utilized in our analysis. This dataset lays a foundation for a detailed examination of ACL ruptures.

3 Methodology

3.1 Pipeline

The pipeline of our model is shown in Figure 2, consisting of two feature extraction branches, a feature fusion stage and the final linear classification layer. Note that the feature extract branch is not restricted to any specific model. Various methods capable of processing 3D image data and point cloud data can also function as feature extraction module.

3.2 CNN for MRI series

Our approach to analyzing MRI series employs the 3D-DenseNet [23] architecture. This architecture is particularly effective because it builds a rich, layered

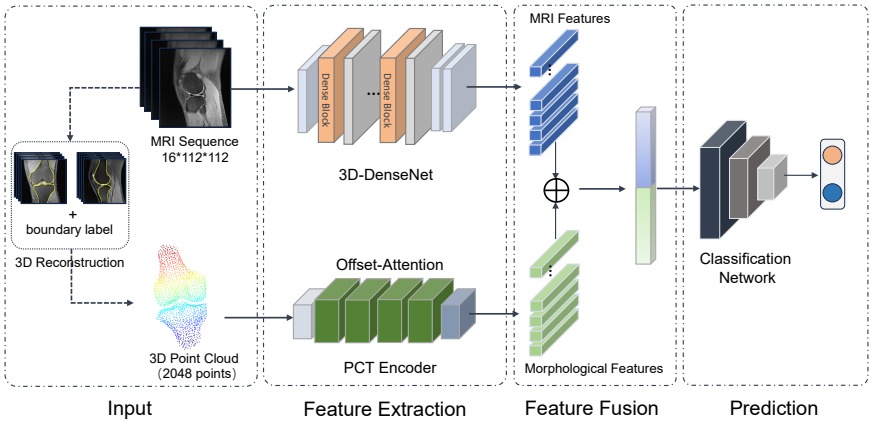

Fig. 2. ACLNet's pipeline, which accepts two inputs of MRI image sequences and point clouds, consists of two feature extraction branches, a feature fusion module, and a linear classification layer.

understanding of the MRI data. In 3D-DenseNet, each layer does not operate in isolation on its input. It rather integrates the outputs from all previous layers, continually enhancing its overall representation of the MRI images. Between these dense blocks, transition blocks help manage the network's complexity by compressing the data, ensuring the model remains efficient and focused. By leveraging the comprehensive feature integration offered by 3D-DenseNet, we lay a solid foundation for accurate diagnosis. We denote this image feature extraction component as F_{im}. Given an MRI sequence input X_i, its MRI features $f_i^{im} \in \mathbb{R}$ are represented as:

$$f_i^{im} = F_{im}(X_i) \tag{1}$$

3.3 Transformer for point cloud

For analyzing point cloud, we apply the Point Cloud Transformer (PCT) [6] method, which adapts the foundational Transformer model to suit point cloud data. PCT innovates by introducing an Offset Attention (OA) module akin to the discrete Laplacian operator used in Graph Convolutional Networks (GCN) [5], replacing the standard Self-Attention (SA) mechanism. Drawing inspiration from PointNet++ [13] and DGCNN [20], PCT further boosts its local feature extraction capabilities through neighbor point embedding. This dual focus on global and local features makes PCT exceptionally adept at parsing the intricate structures of point clouds. Let this image feature extraction branch named F_{pc}, given a point cloud input P_i, its MRI features $f_i^{pc} \in \mathbb{R}$ is represented as:

$$f_i^{pc} = F_{pc}(P_i) \tag{2}$$

3.4 Feature fusion

For the integration of image and point cloud features, we perform feature fusion at the feature level after extracting linear feature values from both modalities. This fusion process employs techniques like concatenation, weighted addition, and cross-attention to effectively blend the diverse data types. Concatenate approach works best due to the inherent disparities in data derived from different sources, we primarily opt for concatenation along the feature dimension as our fusion strategy. We extracted 128-dimensional image features and 256-dimensional point cloud morphological features before the linear fc layer of 3D-DenseNet and PCT branches. Given image feature $f_i^{im} \in \mathbb{R}$ and point cloud feature $f_i^{pc} \in \mathbb{R}$, we obtain the global instance feature $f_i \in \mathbb{R}$ as follows:

$$f_i = f_i^{im} \oplus f_i^{pc} \tag{3}$$

Following concatenation, two fully connected layer, which we named as L, is introduced to process the combined feature set, culminating in the model's final prediction output:

$$\hat{y}_i = L(f_i) \tag{4}$$

This fusion approach ensures a comprehensive representation of the data, leveraging both global and local insights to enhance diagnostic accuracy.

4 Experiments

4.1 Implementation details

In our experimental framework, we adopt the cross-entropy loss function to guide all training processes

$$\mathcal{L}_{cls}(y_i, \hat{y}_i) = \frac{1}{N} \sum_{i=1}^{N} \left[y_i \ln \left(\hat{y}_i \right) + (1 - y_i) \ln \left(1 - \hat{y}_i \right) \right] \tag{5}$$

where $\hat{y}_i$ is the model prediction for sample i. Optimization of the model parameters is conducted using the Adam optimizer and the learning rate is meticulously set at 0.0001. We structured the training regimen to span 200 epochs and set the batch size to be 32. All computational tasks were executed on a setup consisting of four RTX 2080s graphics cards.

4.2 Results

Our analysis of the model's classification capabilities utilized a comprehensive set of metrics, including accuracy (Acc), area under the curve (Auc), precision (Prec), sensitivity (Sens), specificity (Spec), and F1 score (F1). Given the absence of publicly accessible datasets tailored for ACL classification tasks, our experimentation relied on the dataset described in Section 2. In addition to 3D-DenseNet [23], we benchmarked our approach against other image-series-based

Table 2. Evaluational Metrics of Compared Methods for ACL Rupture Classification.

Method	*Acc*↑	*Auc*↑	*Prec*↑	*Sens* ↑	*Spec* ↑	*F*1 ↑
Reports by experts	**92.73**	-	**92.59**	**95.45**	90.53	**92.69**
MRNet [3]	79.90	87.54	79.92	78.65	81.15	79.89
MRNet [3] + PCT [6]	90.63	95.38	90.46	<u>92.62</u>	87.85	90.34
3D-DenseNet [23]	87.59	93.63	87.23	89.40	85.05	87.23
Ours	<u>92.57</u>	**96.57**	<u>92.14</u>	90.67	**95.28**	<u>92.44</u>

methodologies, notably MRNet [3]. We augmented these comparisons by incorporating point cloud data to assess the impact on classification outcomes. The summarized results are presented in Table 2. The integration of bone morphology point cloud data heralds a significant improvement across all metrics. The augmented model achieves its best performance with AUC, reaching 96.57%. Moreover, it demonstrates significant progress in other metrics, effectively matching the accuracy of manual diagnoses. These results underscore the transformative impact of integrating bone morphological data into the ACL classification process, affirming its efficacy in enriching the model's diagnostic potential.

4.3 Ablation study

Our study delves into the contributions of different modules to feature extraction, exploring the impact of various feature fusion methods and point cloud sampling points on the results. The findings, summarized in Table 3, unveil a pivotal insight: relying solely on either image sequences or point cloud yields an accuracy just above 80%. However, the fusion of these two data types remarkably elevates accuracy to 90%, underscoring the synergistic relationship between bone morphology and image data in ACL classification. Among the fusion methods evaluated, the concatenate approach emerges as the most effective. To balance the trade-off between performance and computational efficiency, we set the sampling number to 2048 in most experiments. The concatenate fusion approach not only enhances model performance but also streamlines the integration of complex diagnostic criteria into a cohesive assessment framework.

4.4 Manual annotated points vs. Auto generated points

To validate the efficacy of our classification approach, we conducted a preliminary study. Initially, our input point clouds relied on in-house annotations. However, we aimed to automate this process by deploying a segmentation model called U2Net [14]. Following the original setup, we trained the U2Net model and generated segmentation masks for the validation set. Then, we employed the same point sampling techniques, as described in Section 2, to construct the point cloud from the automatic segmentation result. The results, detailed in Table 4 and illustrated in Figure 3, indicate a modest discrepancy between

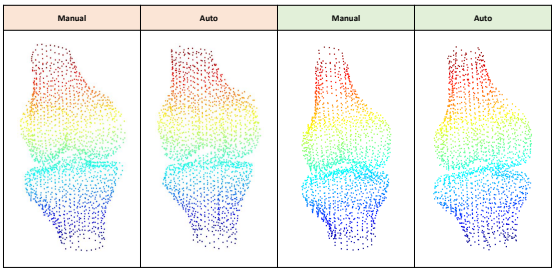

Fig. 3. Two samples of automatically generated point cloud versus manually annotated point cloud.

Table 3. Ablation Study for Components of ACLNet ($\oplus$: Concatenate, $+$: Weighted Sum, $\otimes$: Attention).

Method	Sample Points	Feature fusion	*Acc*↑	*Auc*↑	*Prec*↑	*Sens*↑	*Spec*↑	*F*1↑
3D-DenseNet [23]	-	-	87.59	93.63	87.23	89.40	85.05	87.23
PCT [6]	-	-	84.38	90.87	85.00	91.10	77.72	84.31
ACLNet	2048	$\otimes$	90.62	96.69	90.13	90.07	91.43	90.39
ACLNet	2048	$+$	90.62	**97.48**	90.20	91.17	94.34	90.48
ACLNet	2048	$\oplus$	**92.57**	96.57	**92.14**	90.67	**95.28**	**92.44**
ACLNet	1024	$\oplus$	88.20	92.12	85.83	88.67	86.79	86.98
ACLNet	4096	$\oplus$	89.84	94.77	90.03	**94.00**	83.96	89.41

manually annotated and automatically generated point clouds. Especially when 3D-DenseNet [23] serves as the image sequence feature extractor, our generated point data achieves a consistent results versus manual generated point data on all indicators. Although the point cloud generated by segmentation combined with MRNet [3] cannot catch up with the result of manual annotation, it also gains considerable performance improvement compared with solely image branches, boosting the standard accuracy by 7.57%. It's imperative to highlight that the enhancement in results is directly correlated with the segmentation model's proficiency. This methodology holds the potential to evolve into a fully automated, end-to-end training paradigm.

5 Conclusion

In this study, we introduce ACLNet, an innovative approach for diagnosing anterior cruciate ligament (ACL) injuries. Inspired by extensive clinical experience and prior biomechanics research, this method distinguishes itself from previous deep learning efforts by incorporating bone morphology—a factor can hardly percieved by human—into the model training process. Experimental results demonstrates significant performance improvement versus image-only methods, showing our model is comparable to human experts.

Table 4. Comparison of results on MRI datasets without bone boundary labeling($\star$ represents point clouds generated automatically).

Method	$Acc\uparrow$	$Auc\uparrow$	$Prec\uparrow$	$Sens\uparrow$	$Spec\uparrow$	$F1\uparrow$
MRNet [3]	79.90	87.54	79.92	78.65	81.15	79.89
MRNet [3] + PCT [6]	90.63	95.38	90.46	92.62	87.85	90.34
MRNet [3] + PCT [6]$\star$	86.33	93.89	85.98	88.59	83.18	85.93
3D-DenseNet [23]	87.59	93.63	87.23	89.40	85.05	87.23
Ours	92.57	96.57	92.14	90.67	95.28	92.44
Ours$\star$	92.58	96.61	92.18	90.60	95.33	92.45

In medical imaging tasks, collaboration between computer method developers and clinicians is crucial. By combining clinical insights with deep learning tools, we can improve diagnostic capabilities and deepen our understanding of disease mechanisms within the interconnected human body.

Acknowledgments. This work was supported by Sino-German Center (M 0187), the Natural Science Foundation of China under contract 62088102, and the science and technology innovation special fund of Beijing, China (HDCXZHZB2023201).

Disclosure of Interests. The authors have no competing interests to declare that are relevant to the content of this article

References

1. Al-Saeed, O., Brown, M., Athyal, R., Sheikh, M.: Association of femoral intercondylar notch morphology, width index and the risk of anterior cruciate ligament injury. Knee Surgery, Sports Traumatology, Arthroscopy **21**, 678–682 (2013)
2. Bayer, S., Meredith, S.J., Wilson, K.W., Pauyo, T., Byrne, K., McDonough, C.M., Musahl, V., et al.: Knee morphological risk factors for anterior cruciate ligament injury: a systematic review. The Journal of Bone & Joint Surgery **102**(8), 703–718 (2020)
3. Bien, N., Rajpurkar, P., Ball, R.L., Irvin, J., Park, A., Jones, E., Bereket, M., Patel, B.N., Yeom, K.W., Shpanskaya, K., et al.: Deep-learning-assisted diagnosis for knee magnetic resonance imaging: development and retrospective validation of mrnet. PLoS Medicine **15**(11), e1002699 (2018)
4. Bongbong, D.N., Oeding, J.F., Ma, C.B., Pedoia, V., Lansdown, D.A.: Posterior tibial slope, notch width, condylar morphology, trochlear inclination, and tibiofemoral mismatch predict outcomes following anterior cruciate ligament reconstruction. Arthroscopy: The Journal of Arthroscopic & Related Surgery **38**(5), 1689–1704 (2022)
5. Bruna, J., Zaremba, W., Szlam, A., LeCun, Y.: Spectral networks and locally connected networks on graphs. arXiv preprint arXiv:1312.6203 (2013)
6. Guo, M.H., Cai, J.X., Liu, Z.N., Mu, T.J., Martin, R.R., Hu, S.M.: PCT: Point cloud transformer. Computational Visual Media **7**, 187–199 (2021)

7. Imhoff, F.B., Mehl, J., Comer, B.J., Obopilwe, E., Cote, M.P., Feucht, M.J., Wylie, J.D., Imhoff, A.B., Arciero, R.A., Beitzel, K.: Slope-reducing tibial osteotomy decreases acl-graft forces and anterior tibial translation under axial load. Knee Surgery, Sports Traumatology, Arthroscopy **27**, 3381–3389 (2019)
8. Kunze, K.N., Rossi, D.M., White, G.M., Karhade, A.V., Deng, J., Williams, B.T., Chahla, J.: Diagnostic performance of artificial intelligence for detection of anterior cruciate ligament and meniscus tears: A systematic review. Arthroscopy: The Journal of Arthroscopic & Related Surgery **37**(2), 771–781 (2021)
9. Micicoi, G., Jacquet, C., Khakha, R., LiArno, S., Faizan, A., Seil, R., Kocaoglu, B., Cerciello, S., Martz, P., Ollivier, M.: Femoral and tibial bony risk factors for anterior cruciate ligament injuries are present in more than 50% of healthy individuals. The American Journal of Sports Medicine **49**(14), 3816–3824 (2021)
10. Misir, A., Uzun, E., Sayer, G., Guney, B., Guney, A.: Anatomic factors associated with the development of an anterior cruciate ligament rerupture in men: a case-control study. The American Journal of Sports Medicine **50**(12), 3228–3235 (2022)
11. Namiri, N.K., Flament, I., Astuto, B., Shah, R., Tibrewala, R., Caliva, F., Link, T.M., Pedoia, V., Majumdar, S.: Deep learning for hierarchical severity staging of anterior cruciate ligament injuries from MRI. Radiology: Artificial Intelligence **2**(4), e190207 (2020)
12. Pedoia, V., Norman, B., Mehany, S.N., Bucknor, M.D., Link, T.M., Majumdar, S.: 3D convolutional neural networks for detection and severity staging of meniscus and pfj cartilage morphological degenerative changes in osteoarthritis and anterior cruciate ligament subjects. Journal of Magnetic Resonance Imaging **49**(2), 400–410 (2019)
13. Qi, C.R., Yi, L., Su, H., Guibas, L.J.: Pointnet++: Deep hierarchical feature learning on point sets in a metric space. Advances in Neural Information Processing Systems **30** (2017)
14. Qin, X., Zhang, Z., Huang, C., Dehghan, M., Zaiane, O.R., Jagersand, M.: U2-net: Going deeper with nested u-structure for salient object detection. Pattern Recognition **106**, 107404 (2020)
15. Qu, C., Yang, H., Wang, C., Wang, C., Ying, M., Chen, Z., Yang, K., Zhang, J., Li, K., Dimitriou, D., et al.: A deep learning approach for anterior cruciate ligament rupture localization on knee mr images. Frontiers in Bioengineering and Biotechnology **10**, 1024527 (2022)
16. Sanders, T.L., Maradit Kremers, H., Bryan, A.J., Larson, D.R., Dahm, D.L., Levy, B.A., Stuart, M.J., Krych, A.J.: Incidence of anterior cruciate ligament tears and reconstruction: a 21-year population-based study. The American Journal of Sports Medicine **44**(6), 1502–1507 (2016)
17. Vaswani, A., Shazeer, N., Parmar, N., Uszkoreit, J., Jones, L., Gomez, A.N., Kaiser, Ł., Polosukhin, I.: Attention is all you need. Advances in Neural Information Processing Systems **30** (2017)
18. Wang, D., Kent III, R.N., Amirtharaj, M.J., Hardy, B.M., Nawabi, D.H., Wickiewicz, T.L., Pearle, A.D., Imhauser, C.W.: Tibiofemoral kinematics during compressive loading of the ACL-intact and ACL-sectioned knee: roles of tibial slope, medial eminence volume, and anterior laxity. The Journal of Bone & Joint Surgery **101**(12), 1085–1092 (2019)
19. Wang, D.y., Liu, S.g., Ding, J., Sun, A.l., Jiang, D., Jiang, J., Zhao, J.z., Chen, D.s., Ji, G., Li, N., et al.: A deep learning model enhances clinicians' diagnostic accuracy to more than 96% for anterior cruciate ligament ruptures on magnetic resonance imaging. Arthroscopy: The Journal of Arthroscopic & Related Surgery **40**(4), 1197–1205 (2024)

20. Wang, Y., Sun, Y., Liu, Z., Sarma, S.E., Bronstein, M.M., Solomon, J.M.: Dynamic graph CNN for learning on point clouds. ACM Transactions on Graphics (TOG) **38**(5), 1–12 (2019)
21. Whittaker, J.L., Losciale, J.M., Juhl, C.B., Thorlund, J.B., Lundberg, M., Truong, L.K., Miciak, M., Van Meer, B.L., Culvenor, A.G., Crossley, K.M., et al.: Risk factors for knee osteoarthritis after traumatic knee injury: a systematic review and meta-analysis of randomised controlled trials and cohort studies for the optiknee consensus. British Journal of Sports Medicine **56**(24), 1406–1421 (2022)
22. Yu, B., Garrett, W.E.: Mechanisms of non-contact acl injuries. British Journal of Sports Medicine **41**(suppl 1), i47–i51 (2007)
23. Zhang, J., Lu, C., Li, X., Kim, H.J., Wang, J.: A full convolutional network based on densenet for remote sensing scene classification. Mathematical Biosciences and Engineering **16**(5), 3345–3367 (2019)